A NEW WAVELET–BASED EDGE DETECTOR VIA CONSTRAINED OPTIMIZATION

Hong–Yuan Mark Liao† [1], Ming–Tat Ko†, Jun–Wei Hsieh‡, and Kuo–Chin Fan‡

†Institute of Information Science, Academia Sinica, Taiwan

‡Institute of Computer Science and Electronic Engineering

National Central University, Chung–Li, Taiwan

email: liao@iis.sinica.edu.tw

Tel: +886(2)788–3799 ext. 2413

Fax: +886(2)782–4814

Abstract

This report proposes a new wavelet–based approach to solving the edge detection problem. The proposed scheme adopts Canny's three criteria [3] as a guide to derive a wavelet–style edge filter such that the edge points of an image can be detected efficiently and accurately at different scales. Since Canny's criteria are suitable for those edge detectors that detect local extremes, the desired wavelet is therefore chosen to be anti–symmetric. In order to reconstruct the original image, the dual of the desired wavelet is also required. Basically, the pair of wavelets are represented as linear combinations of translations of a scaling function. By introducing a constrained optimization process, the set of expansion coefficients of the desired wavelet and its dual as well, can be determined. In order to implement the desired edge detector, a continuous wavelet has to be converted into the discrete form. For this purpose, the format of the discrete wavelet transform has to be developed. Since the proposed edge filter is wavelet–based, the inherent multi-resolution nature of wavelet transform provides more flexibility in the analysis of images. Also, since an optimization process is introduced in the filter derivation process, the performance of the proposed filter is better than that of Mallat–Zhong's edge detector. In real implementation, the experimental results show that the proposed approach is indeed superb.

Keywords: edge detection, wavelet transform, constrained optimization.

---

[1] To whom all correspondence should be addressed.

[2] This work is partially supported by the National Science Council of Taiwan under Grant NSC 84–2213–E–001–008.

I. Introduction

Digital edge detection is an important early vision process for reducing the amount of data in raw images to facilitate the subsequent high–level image understanding tasks. It has been of interest to research in the area of computer vision from the outset[1]–[23]. In [1], Marr and Hildreth proposed an important zero–crossing detection technique. They introduced a new method to process an image by applying Laplacian of Gaussian filters characterized by different variances. In [3], Canny used a smoothed gradient method to locate points with extreme values in an image as edge points. In his approach, edge detection is characterized as a constrained optimization process which has to fulfill three criteria. The three criteria are **good detection**, **good localization**, and **low spurious response.** The filter he obtained is equivalent to performing a Gaussian filtering followed by a gradient detection. Edge operators which are similar to this kind can be found in [4], [5], [10]–[14]. Another important solution for edge detection is to solve the problem by using spatial frequency response. Researchers in this aspect designed optimal edge filters in the frequency domain [15]–[18]. In [19]–[20], an image was modeled as a random field and the pixels with abrupt changes of statistical properties were detected as edge points. Recently, a new edge filter based on wavelet transform has been proposed by Mallat and Zhong [4]. They combined the properties of wavelet transform and a gradient method to form a ''multi–scale'' edge detector. In their work, the first derivative of a cubic spline function is utilized to detect the local extreme values of a wavelet transform as edge points. However, the ultimate goal of the work is to efficiently compress the input image. Therefore, although the adopted wavelet is capable of detecting edges, the performance of edge detection was not a major concern in their work.

Basically, wavelet is a basis of functions that can be applied to efficiently and accurately represent ''things''. The thing could be a signal, system, process or physical phenomenon. A wavelet basis can be orthonormal or non–orthogonal. The orthogonal wavelet bases have been successfully used in applied mathematics [29]– [30] and digital signal processing [29]. However, for some applications, especially in edge detection, the orthonormality of wavelet basis is a strict limitation on designing an efficient edge filter [4], [5], [29]. Torre and Poggio[7] pointed out that if an edge detector is to detect the zero–crossings of output as edge points, it must be symmetric with respect to the origin. On the other hand, if an edge detector is to detect the local extreme as edge points, it must be anti–symmetric with respect to the origin. In this report, we propose a scheme with Canny's criteria as a guide to derive a wavelet–style edge filter such that

the edge points of an image can be detected efficiently and accurately at different scales. Since Canny's criteria are suitable for those edge detectors that detect local extremes, the desired wavelet is therefore chosen to be anti–symmetric. In order to obtain the information for reconstructing the original image and to avoid the orthonormality constraint of a wavelet, the dual of the derived wavelet is also required. Basically, the pair of wavelets, i.e., the desired wavelet and its dual, are represented as linear combinations of translations of a scaling function. In this report, the quadratic spline function and the cubic one, respectively, are adopted as a scaling function to expand the desired filter. By introducing a constrained optimization process, the set of coefficients of the desired wavelet and that of its dual one as well, can be determined. In order to implement the desired edge detector, a continuous wavelet has to be converted into the discrete form. For this purpose, the format of the discrete wavelet transform has to be developed. In sum, the proposed edge filter is similar to a gradient edge detector. Since it is wavelet–based, the inherent multiresolution nature of wavelet transform provides more flexibility in the analysis of images. Also, since an optimization process is introduced in the filter derivation process, the performance of the proposed filter is better than that of Mallat–Zhong's edge detector. In real implementation, the experimental results show that the proposed approach is indeed superb.

In what follows, the relations between edge detection and non–orthogonal wavelet transform will be introduced in Section II. Then, in Section III, the three criteria for designing an optimal edge filter proposed by Canny are briefly described. The detailed procedure for designing a near optimal edge filter is elaborated in Section IV. In Section V, the derived filter is extended to 2–D and its dual wavelet is determined. Section VI reports some experimental results and Section VII concludes the work with some discussions.

II. Edge Detection and Non − Orthogonal Wavelet Transform

Wavelet transform (WT) [25] for multiresolution local analysis on signals has been proved to be very effective. It has been successfully applied to image compression, signal detection such as speech, seismic, biomedical, and other signals. The format of a WT, based on its supporting basis, can be categorized into two classes, i.e., the orthonormal basis and the non–orthogonal one. It has been pointed out that the orthonormal scheme is not a must in deriving a good edge detector [4], [5], [29]. There were a number

of researchers who designed their edge detectors based on non–orthogonal wavelet bases [4], [5], [29]. In what follows, the model of wavelet bases is described.

Some notations which will be used throughout the report will be elaborated. All the functions considered here are in $L^2(R)$, the space of square–integrable functions over real numbers. For *f(x)* and *g(x)* in $L^2(R)$, the inner product $< f(x), g(x) > = \int f(x)g(x)dx$ and the convolution $f(x) * g(x) = \int f(u)$ $g(x-u)du$. The Fourier transform of *f(x)* is denoted by $\hat{f}(\omega) = \int f(x)e^{-i\omega x}dx$. The scaled function, $\frac{1}{s}\psi(\frac{x}{s})$, of $\psi(x)$ is denoted by $\psi_s(x)$. A wavelet is a function $\psi(x) \in L^2(R)$ satisfying the admissibility condition $C_\psi = \int \frac{|\hat{\psi}(\omega)|^2}{|\omega|}d\omega < \infty$. A continuous wavelet transform of a signal *f(x),* with wavelet $\psi(x)$, is

$$\begin{aligned} W_s f(x) &= < f(u), \frac{1}{s}\psi(\frac{x-u}{s}) > = < f(u), \psi_s(x-u) > \\ &= f * \psi_s(x). \end{aligned} \tag{1}$$

From the Fourier transform of Equation (1), we have

$$\hat{W}_s f(\omega) = \hat{f}(\omega)\hat{\psi}(s\omega).$$

The dyadic wavelet transform of *f(x)* is:

$$W_{2^j} f(x) = f * \psi_{2^j}(x), \tag{2}$$

for scale parameter $s = 2^j$ for $j \in Z$. Furthermore, if there exists two strictly positive constants ϱ_1 and ϱ_2 such that

$$\forall\ \omega \in R,\ \varrho_1 \leq \sum_{j=-\infty}^{\infty} |\hat{\psi}(2^j\omega)| \leq \varrho_2, \tag{3}$$

then $\psi(x)$ has a dual wavelet $\xi(x)$, by which the signal *f(x)* can be reconstructed as follows:

$$f(x) = \sum_{j=-\infty}^{\infty} W_{2^j} f(x) * \xi_{2^j}(x). \tag{4}$$

From the Fourier transform of Equation (4), we have

$$\sum_{j=-\infty}^{\infty} \hat{\psi}(2^j\omega)\hat{\xi}(2^j\omega) = 1. \tag{5}$$

Let $\phi(x)$ denote the scaling function whose Fourier transform is an aggregation of $\hat{\psi}(2^j\omega)$ and $\hat{\xi}(2^j\omega)$ for $j \geq 1$, i.e.,

$$|\hat{\phi}(\omega)|^2 = \sum_{j=1}^{\infty} \hat{\psi}(2^j\omega)\hat{\xi}(2^j\omega). \tag{6}$$

A direct implication of Equation (6) is

$$|\hat{\phi}(2^{j-1}\omega)|^2 - |\hat{\phi}(2^j\omega)|^2 = \hat{\psi}(2^j\omega)\hat{\xi}(2^j\omega). \quad (7)$$

Equation (7) illustrates the relations among $\phi(x)$, $\psi(x)$ and $\xi(x)$ at different scales. If the scaling function $\phi(x)$ and the wavelet function $\psi(x)$ are determined beforehand, based on Equation (7), the corresponding dual wavelet $\xi(x)$ can be derived.

Let S_{2^j} be the smoothing operator with respect to the scaling function $\phi(x)$ defined by

$$S_{2^j}f(x) = f(x) * \phi_{2^j}(x). \quad (8)$$

Suppose that *f(x)* is defined at the finest resolution, i.e., $f(x) = S_{2^0}f(x)$. By using the scaling function $\phi(x)$ and the wavelet function $\psi(x)$, a signal *f(x)* can be decomposed into different components $\left\{S_{2^j} f(x)\right\}_{j=1,2,..}$ and $\left\{W_{2^j} f(x)\right\}_{j=1,2,..}$. $S_{2^j} f(x)$ is an approximation view of *f(x)* at scale 2^j and $W_{2^j} f(x)$ the difference between $S_{2^{j-1}} f(x)$ and $S_{2^j} f(x)$. If $\phi(x)$ and $\psi(x)$ are considered respectively as the low–pass and high–pass filter, then $S_{2^j} f(x)$ is equivalent to the low frequency component of *f(x)* at scale 2^j and $W_{2^j} f(x)$ the high frequency component, i.e., the edge information of *f(x)* at scale 2^j. Therefore, by using the information of $\left\{S_{2^j} f(x)\right\}_{j=1,2,..}$ and $\left\{W_{2^j} f(x)\right\}_{j=1,2,..}$, the original function can be reconstructed. The reconstruction is a recursive process based on Equation (7). Multiplying both sides of Equation (7) by $\hat{f}(\omega)$ and taking the inverse Fourier transform, we obtain

$$S_{2^{j-1}}f(x) * \overline{\phi}_{2^{j-1}}(x) = S_{2^j}f(x) * \overline{\phi}_{2^j}(x) + W_{2^j}f(x) * \xi_{2^j}(x), \quad (9)$$

where $\overline{\phi}(x) = \phi(-x)$. By Equation (9), $S_{2^{j-1}} f(x)$ can be recovered from $S_{2^j} f(x)$ and $W_{2^j} f(x)$. Applying the above process recursively, the original signal, $f(x) = S_{2^0} f(x)$, can be reconstructed.

In the previous contents, $S_{2^j} f(x)$ is known as an approximation scheme of *f(x)* at scale 2^j, where $S_{2^j} f(x)$ is a better approximation of *f(x)* than $S_{2^{j+1}} f(x)$ for $j \in Z^+$, and $W_{2^j} f(x)$ the edge information of *f(x)* at the scale 2^j [4], [26]. It has been proved that the multi–scale edge information can provide a complete and stable description of a signal[8]. Based on this concept, Mallat and Zhong [4] introduced a very efficient multi–scale method which uses the extremes of wavelet transform to represent an image. This method only needs low algorithmic complexity and produces accurate reconstruction results. Let $W_{2^j} f(n)$ be the discrete form of $W_{2^j} f(x)$. If the edge points are selected by detecting the zero–crossings of $W_{2^j} f(n)$, then this wavelet transform is equivalent to a Marr–Hildreth edge detector [1]; while if we denote the local extreme of $W_{2^j} f(n)$ as edge points, it corresponds to a Canny edge detector [3]. The wavelet,

proposed by Mallat and Zhong, is a Canny–style edge detector. In this report, we propose a scheme, which integrates the properties of wavelet transform and Canny's criteria, to derive a wavelet and its corresponding dual wavelet for efficiently detecting edge points and reconstructing original image.

In the derivation of the desired wavelet, both the quadratic and cubic spline functions are chosen as scaling functions. The scaling function, $\phi(x)$, in the frequency domain can be written as follows[4]:

$$\hat{\phi}(\omega) = e^{-i\beta_1\omega} \prod_{m=1}^{\infty} H(2^{-m}\omega), \tag{10}$$

where $H(\omega)$ is a 2π periodic differentiable function satisfying

$$|H(\omega)|^2 + |H(\omega + \pi)|^2 \leq 1 \text{ and } H(0) = 1. \tag{11}$$

The parameter, $0 \leq \beta_1 < 1$, is a sampling shift. With the form in Equation (10), we have

$$\hat{\phi}(2\omega) = e^{-i\beta_1\omega} H(\omega)\hat{\phi}(\omega). \tag{12}$$

As in [4], we may impose further that the Fourier transform of the desired wavelet $\psi(x)$ and its dual wavelet $\xi(x)$ are:

$$\hat{\psi}(2\omega) = e^{-i\beta_2\omega} G(\omega)\hat{\phi}(\omega), \tag{13}$$

and

$$\hat{\xi}(2\omega) = e^{i\beta_2\omega} K(\omega)\hat{\phi}(\omega), \tag{14}$$

where $G(\omega)$ and $K(\omega)$ are two 2π periodic differentiable functions and $0 \leq \beta_2 < 1$ is another sampling shift. Plugging Equations (12)–(14) into Equation (7), since $\phi(x)$ is symmetric with respect to 0, we have

$$|H(\omega)|^2 + G(\omega)K(\omega) = 1. \tag{15}$$

It can be proved that if $H(\omega)$, $G(\omega)$ and $K(\omega)$ satisfy Equations (10) and (15), $\hat{\phi}(2\omega)$, $\hat{\psi}(2\omega)$ and $\hat{\xi}(2\omega)$ defined in Equations (12)–(14) will satisfy Equation (7). In general, $H(\omega)$ is determined in advance, and $G(\omega)$ is adjusted to satisfy the requirements of a specified application. Therefore, once $H(\omega)$ and $G(\omega)$ are known, $K(\omega)$ can be obtained by solving Equation (15) and $\xi(x)$ can be determined by Equation (14).

The three 2π periodic functions $H(\omega)$, $G(\omega)$ and $K(\omega)$ can be expanded respectively as follows:

$$H(\omega) = \sum_{n=-\infty}^{\infty} h(n)e^{-in\omega},\ G(\omega) = \sum_{n=-\infty}^{\infty} g(n)e^{-in\omega} \text{ and } K(\omega) = \sum_{n=-\infty}^{\infty} k(n)e^{-in\omega},$$

where $\{h(n)\}_{n\in Z}$, $\{g(n)\}_{n\in Z}$ and $\{k(n)\}_{n\in Z}$ are three real sequences satisfying

$$\sum_{n=-\infty}^{\infty} |h(n)|^2 < \infty,\ \sum_{n=-\infty}^{\infty} |g(n)|^2 < \infty \text{ and } \sum_{n=-\infty}^{\infty} |k(n)|^2 < \infty.$$

Plugging the above expansions into Equations (12)–(14) and taking their inverse Fourier transforms, we obtain

$$\frac{1}{2}\phi(\frac{x}{2}) = \sum_{n=-\infty}^{\infty} h(n)\phi(x - n - \beta_1), \tag{16}$$

$$\frac{1}{2}\psi(\frac{x}{2}) = \sum_{n=-\infty}^{\infty} g(n)\phi(x - n - \beta_2), \tag{17}$$

$$\text{and } \frac{1}{2}\xi(\frac{x}{2}) = \sum_{n=-\infty}^{\infty} k(n)\phi(x - n + \beta_2). \tag{18}$$

Equations (16)–(18) indicate that $\frac{1}{2}\phi(\frac{x}{2})$, $\frac{1}{2}\psi(\frac{x}{2})$ and $\frac{1}{2}\xi(\frac{x}{2})$ can all be considered as the linear combinations of $\phi(x - n - \beta)$, where β is a constant shift. In general cases, the shift constants $\{\beta_i\}_{i=1,2}$ are set to 0. However, in some special cases, by adjusting β_1 and β_2 will make the coefficients $\{h(n)\}_{n\in Z}$, $\{g(n)\}_{n\in Z}$ and $\{k(n)\}_{n\in Z}$ converge to zero quickly as $n \to \infty$.

III. Criteria for Optimal Edge Detection

Before a good edge filter is designed, one has to know what criteria are needed to evaluate the performance of an edge filter. In this section, the three criteria proposed by Canny[3] which can be used in evaluating the performance of an edge detector are briefly introduced. In his brilliant approach, edge detection is characterized as an optimization problem which has to fulfill three criteria. The three criteria include **good detection, good localization,** and **low spurious response.** Canny [3] converted the above three conceptual criteria into practical rules. First, the good detection criterion is converted into the detection of a high signal–to–noise ratio. Second, the good localization criterion is equivalent to obtaining a low mean–squared deviation value of the detected edges. Third, the filter should delete spurious edges. Let *f(x)* be a step edge with *f(x)* = 1 when $x \geq 0$, and *f(x)*=0 otherwise. Assume the desired filter is $\psi(x)$ and the response of $\psi(x)$ to *f(x)* at *x* is $R_\psi(x)$. Let *N(x)* be the Gaussian white noise in *f(x)* and $R_N(x)$ the response of the noise. If ϱ^2 represents the variance of *N(x)*, then the signal–to–noise ratio can be defined as follows [3]:

$$\text{SNR} = \frac{R_\psi(0)}{R_N} = \frac{\left| \int_{-\infty}^{\infty} f(-x)\psi(x)\, dx \right|}{\varrho \sqrt{\int_{-\infty}^{\infty} \psi^2(x)dx}} = \Sigma(\psi). \tag{19}$$

As to the second criterion, good localization, Canny defined it as follows [3]:

$$\text{Localization} = \frac{\left| \int_{-\infty}^{\infty} f'(x)\psi'(x)dx \right|}{\varrho \sqrt{\int_{-\infty}^{\infty} \psi'^2(x)dx}} = \Lambda(\psi'). \tag{20}$$

As to the third criterion, Canny stated that the edge filter should not produce spurious maxima in response to a single edge. That is, there is a need to limit the number of peaks of the filter output within the filter's spatial spread. The mean distance, x_{mean}, between peaks in the noise response of $\psi(x)$, using a result due to Rice [32] , can be expressed as follows:

$$x_{mean} = 2\pi \left[\frac{\int_{-\infty}^{\infty} \psi'^2(x)\ dx}{\int_{-\infty}^{\infty} \psi''^2(x)dx} \right]^{\frac{1}{2}} = KW,$$

where x_{mean} is set as some fraction K of the operator width . In [32], the value of W is not well defined. Therefore, Canny[3] made a rough estimate of K for the probability of a spurious edge as follows:

$$K(\psi) = \frac{|\psi'(0)| \left[\int_{-\infty}^{\infty} \psi^2(x)dx \right]^{1/2}}{\left[\int_{-\infty}^{\infty} \psi''^2(x)dx \right]^{1/2} \left| \int_{-\infty}^{0} \psi(x)dx \right|}. \tag{21}$$

Equation (21) is the so–called **multiple response criterion**. Based on the above three criteria, Canny maximized the product of $\Sigma(\psi)\Lambda(\psi')$ and kept $K(\psi)$ constant to obtain his optimal edge detector. Sarkar and Boyer [9] considered the multiple response criterion from another viewpoint. They modified Canny's multiple response criterion as follows[9] :

$$K(\psi) = \left[\frac{\int_{-\infty}^{\infty} \psi'^2(x)dx}{\int_{-\infty}^{\infty} \psi''^2(x)dx} \right]^{1/2} \left[\frac{\int_{-\infty}^{\infty} \psi^2(x)dx}{\int_{-\infty}^{\infty} x^2\psi^2(x)} \right]^{1/2}. \tag{22}$$

In order to avoid confusion, in this report $K_1(\psi)$ and $K_2(\psi)$ represent Canny's and Sarkar–Boyer's multiple response criterion, respectively. In the next section, the detailed procedure for deriving the proposed edge filter will be elaborated.

IV. Derivation of a New Wavelet–Based Edge Filter

In this section, we will derive a new wavelet–based edge filter by an optimization method. Here, we assume that the step edge to be detected is the same as the one described in Section III. Let $\gamma(x)$ denote the desired wavelet that can detect edge points correctly. In order to detect abrupt intensity changes in an image *f(x),* the convolution, $f(x) * \gamma(x)$, should detect the edges from the image.

By Equation (17) with β_2 set to 0, the wavelet $\frac{1}{2}\gamma(\frac{x}{2})$ can be expanded as a linear combination of $\phi(x + n)$'s as follows:

$$\frac{1}{2}\gamma(\frac{x}{2}) = \sum_n c(n)\phi(x + n). \tag{23}$$

Let $\phi(x)$ be symmetric with respect to the origin, i.e., $\phi(x) = \phi(-x)$. In the introduction, we have stated that $\gamma(x)$ has to be anti–symmetric with respect to the origin, therefore

$$c(n) = -c(-n).$$

It means Equation (23) can be rewritten as

$$\frac{1}{2}\gamma(\frac{x}{2}) = \sum_{n=1}^{\infty} c(n)[\phi(x + n) - \phi(x - n)]. \tag{24}$$

In general, the expression in Equation (24) is not satisfactory because it requires many *c(n)*'s to represent the wavelet $\gamma(x)$. For example, if an edge filter $\gamma(x)$ is expressed in the following form:

$$\frac{1}{2}\gamma(\frac{x}{2}) = \phi(x + 1/3) - \phi(x - 1/3),$$

it is obvious that more than two coefficients are needed to expand the desired edge filter $\gamma(x)$. In order to reduce the number of coefficients involved in expressing $\gamma(x)$, a more general form is defined as follows:

$$\frac{1}{2}\gamma(\frac{x}{2}) = \sum_{n=0}^{\infty} c(n)[\phi(x + n + \alpha) - \phi(x - n - \alpha)], \tag{25}$$

where $0 \le \alpha < 1$. Basically, Equation (24) can be considered as a special case of Equation (25). In practice, n cannot vary from 0 to ∞. Under the circumstances, the desired wavelet $\gamma(x)$ can only be approximated by a finite form as follows:

$$\gamma(x) \approx \sum_{n=0}^{N} 2c(n)[\phi(2x + n + \alpha) - \phi(2x - n - \alpha)]. \tag{26}$$

Now, the problem at hand is to solve the set of coefficients $\{c(n)\}_{n=0,1,..,N}$ and α such that $\gamma(x)$ can efficiently and accurately detect edge points of an image *f(x)*. In order to obtain $\{c(n)\}_{n=0,1,..,N}$ and α, a constrained optimization process is introduced. Based on Canny's edge optimality criteria, an objective function is defined as follows:

$$W = \frac{1}{\zeta}, \tag{27}$$

where $\zeta = \Sigma(\gamma) \times \Lambda(\gamma') \times (0.0001 + K(\gamma))$. Here, $\Sigma(\gamma)$ and $\Lambda(\gamma')$ are Canny's good detection and good localization criteria, respectively. $K(\gamma)$ is either Canny's (Equation (21)) or Sarkar–Boyer's (Equation (22)) multiple response criterion. The reason why a small constant, 0.0001, is added to the objective function is to protect the terms in $\Sigma(\gamma)$ and $\Lambda(\gamma')$ from being cancelled out. With the objective function *W*, the resulting coefficients $\{c(n)\}_{n=0,1,..,N}$ may decay very slowly and the requirement of compact support of a wavelet is not satisfied. Under the circumstances, in real implementation, an extra constraint is introduced to guarantee fast decay when the proposed edge filter is applied. Expecting the resulting *c(n)*'s to decay with the rate n^{-2}, the extra constraint is defined as follows:

$$\eta = \sum_{n=1}^{N} \left| \frac{n^2 c(n)}{c(0)} \right|^{\mu}, \tag{28}$$

where μ is an adjustable parameter. Plugging this constraint into the objective function, *W*, a new objective function W' is formed:

$$W' = \frac{\eta}{\zeta}. \tag{29}$$

Based on the objective function defined in Equation (29), a constrained optimization process can be executed. The set of unknown coefficients $\{c(n)\}_{n=0,1,..,N}$ and α can be determined after the process is complete. In [4], Mallat and Zhong chose the quadratic spline function as their scaling function, i.e.,

$$\hat{\phi}(\omega) = \left[\frac{\sin \omega/2}{\omega/2} \right]^3. \tag{30}$$

The Fourier transform of its corresponding wavelet is

$$\hat{\psi}(\omega) = i\omega \left[\frac{\sin \omega/4}{\omega/4} \right]^4. \tag{31}$$

Notice that the selection of Mallat–Zhong's mother wavelet did not introduce any optimization process. In this report, Canny's three optimality criteria [3] for deriving an optimal edge filter are introduced. Based on these criteria, a constrained optimization process is executed to determine the set of expansion coeffi-

cients of the desired edge filter. Here, the quadratic and the cubic spline functions are selected, respectively, as the scaling function to expand $\gamma(x)$. Experimental results show that the quadratic spline function works better than the cubic one. In what follows, the derivation details of $\gamma(x)$ will be elaborated.

In general, the Fourier transform of a spline function $N_m(x)$ is defined as follows:

$$\hat{N}_m(\omega) = e^{-i\frac{m}{2}\omega}\left\{\frac{\sin\omega/2}{\omega/2}\right\}^m.$$

$N_m(x)$ is a quadratic spline function when m=3 and a cubic one when m=4. If $N_m(x)$ shifts $\frac{m}{2}$ to the left, it is symmetric with respect to the origin. The shifted spline function,

$$\hat{\phi}^m(\omega) = \left\{\frac{\sin\omega/2}{\omega/2}\right\}^m, \tag{32}$$

can be used as a scaling function to expand $\gamma(x)$. When m=3, by the inverse Fourier transform, the scaling function is:

$$\phi^3(x) = \begin{cases} x^2/2 + 3x/2 + 9/8, & \text{if } -3/2 \le x < -1/2, \\ 3/4 - x^2, & \text{if } -1/2 \le x < 1/2, \\ x^2/2 - 3x/2 + 9/8, & \text{if } 1/2 \le x < 3/2, \\ 0, & \textit{otherwise}. \end{cases} \tag{33}$$

When m=4, the scaling function is:

$$\phi^4(x) = \begin{cases} (x+2)^3/6, & \text{if } -2 \le x < -1, \\ -x^3/2 - x^2 + 2/3, & \text{if } -1 \le x < 0, \\ x^3/2 - x^2 + 2/3, & \text{if } 0 \le x < 1, \\ (2-x)^3/6, & \text{if } 1 \le x < 2, \\ 0, & \textit{otherwise}. \end{cases} \tag{34}$$

Plugging $\phi^3(x)$ or $\phi^4(x)$ into the objective function, W', the set of unknown coefficients $\{c(n)\}_{n=0,1,..,N}$ and α can be determined by an optimization method. Once the set of coefficients $\{c(n)\}_{n=0,1,..,N}$ and α in $\psi(x)$ are determined with the assistance of Canny's criteria, these coefficients can be plugged back into Equation (26) and the desired optimal filter, $\gamma(x)$, is obtained.

In the derivation process, a quadratic scaling function $\phi^3(x)$ is used as an example. The calculations of the set of integrals and derivatives, including $\int_{-\infty}^{0}\gamma(x)$, $\int_{-\infty}^{\infty}\gamma^2(x)$, $\int_{-\infty}^{\infty}\gamma'^2(x)$, $|\gamma'(0)|$, $\int_{-\infty}^{\infty}\gamma''^2(x)$

and $\int_{-\infty}^{\infty} x^2\gamma^2(x)$ which are needed in the determination of $\Sigma(\gamma)$, $\Lambda(\gamma')$ and $K(\gamma)$ are elaborated in Appendix.

Based on the calculations described in Appendix, $\Sigma(\gamma)$, $\Lambda(\gamma')$, and $K(\gamma)$ can be determined accordingly and the objective function, *W,'* is obtained. In Equation (27), the objective function, *W',* has *N*+2 unknown coefficients, i.e., $\{c(n)\}_{n=0,1,..,N}$ and α, needed to be solved. By applying the quasi–Newton method, $\{c(n)\}_{n=0,1,..,N}$ and α for a near optimal $\gamma(x)$ can be determined. In a number of simulations, the best set of coefficients $\{c(n)\}_{n=0,1,..,N}$ and α for an optimal edge detector based on a quadratic spline function is as follows:

$$\alpha = \frac{1}{2},\ c(0) = 1.915714,\ c(1) = 1.212978,\ c(2) = 0.337216,\ c(3) = 0.092042,$$
$$\text{and } c(n) = 0.0,\ \text{for } n \geq 4. \tag{35}$$

Plugging the above results into Equation (26) and taking the dilated scale 2^j as a variable, the best edge detector can be rewritten as follows:

$$\gamma_{2^j}(x) = \frac{1}{2^{j-1}} \sum_{n=0}^{3} c(n)[\phi(\frac{x}{2^{j-1}} + n + \frac{1}{2}) - \phi(\frac{x}{2^{j-1}} - n - \frac{1}{2})]. \tag{36}$$

m	*solution 1*	*solution 2*	*solution 3*	*solution 4*	*Mallat 's wavelet*
c(0)	*1.915714*	*1.909686*	*1.939113*	*2.001813*	*2.0*
c(1)	*1.212978*	*1.101535*	*1.200166*	*1.095990*	*0.0*
c(2)	*0.337216*	*0.244036*	*0.303512*	*0.230633*	*0.0*
c(3)	*0.092042*	*0.022197*	*–0.000303*	*–0.002869*	*0.0*
c(4)	*0.0*	*0.002861*	*–0.000001*	*–0.000038*	*0.0*
c(5)	*0.0*	*0.0*	*0.000119*	*0.000959*	*0.0*
$\Sigma\Lambda$	*1.326794*	*1.288330*	*1.281402*	*1.274669*	*1.0*
K_1	*0.517765*	*0.527944*	*0.534319*	*0.531151*	*0.547723*
K_2	*2.562118*	*2.624933*	*2.624024*	*2.634735*	*3.035067*
$\Sigma\Lambda K_1$	*0.686967*	*0.680165*	*0.684678*	*0.677042*	*0.547723*
$\Sigma\Lambda K_2$	*3.399403*	*3.382780*	*3.362429*	*3.358416*	*3.035067*

Table 1. Solutions 1–4 are four sets of coefficients obtained from four independent constrained optimization processes. Column 5 illustrates the set of coefficients needed in Mallat–Zhong's [1] approach.

The first four columns of Table 1 illustrate four different sets of simulation results after performing optimization. It is obvious that the best set of coefficients is in column 1. Plugging the best coefficient set into Canny's optimality criteria[3] , the value of the performance index is

$$\Sigma(\gamma)\Lambda(\gamma')K(\gamma) = 0.686967.$$

One thing to be noticed is that different sets of coefficients listed in Table 1 all reach a very stable performance. Most importantly, they improve the performance of Mallat–Zhong's[4] method by roughly about 25% if Canny's multiple response criterion is chosen, i.e., $\Sigma(\gamma)\Lambda(\gamma')K_1(\gamma)$; and 10% if Sarkar–Boyer's multiple response criterion is chosen, i.e., $\Sigma(\gamma)\Lambda(\gamma')K_2(\gamma)$. In order to make comparison, the cubic spline function, $\phi^4(x)$, is also taken as a scaling function. It is unfortunate that the derivation process is much more tedious than the case of quadratic spline function. Here, part of the derived coefficient sets and their corresponding $\Sigma(\gamma)$, $\Lambda(\gamma')$ and $K(\gamma)$ are listed in Table 2. From Table 2, the best set of coefficients $\{c(n)\}_{n=0,1,..,N}$ of an optimal wavelet for edge detection based on a cubic spline function is as follows:

$$\alpha = 1/2,\ c(0) = 1.909686,\ c(1) = 1.215350,\ c(2) = 0.344036,\ c(3) = 0.122197,$$
$$c(4) = 0.028610, \text{and } c(n) = 0.0 \text{ for } n \geq 5. \tag{37}$$

One thing to be noticed is that the optimal solution always appears at $\alpha = 1/2$. Compared with the case of $\phi^3(x)$, the coefficient set $\{c(n)\}_{n=0,1,..,N}$ of $\phi^4(x)$ decays slower than that of $\phi^3(x)$. Besides, in the experiment the usage of $\phi^3(x)$ turns out with more accurate results. Therefore, the quadratic spline function is finally selected as our scaling function.

m	*solution 1*	*solution 2*	*solution 3*
c(0)	*1.909686*	*1.909746*	*1.945367*
c(1)	*1.215350*	*1.101479*	*1.187987*
c(2)	*0.344036*	*0.243926*	*0.304037*
c(3)	*0.122197*	*0.021398*	*0.002662*
c(4)	*0.028610*	*0.0*	*–0.000731*
c(5)	*0.0*	*0.0*	*–0.008827*
$\sum\Lambda$	*1.140802*	*1.072068*	*1.065773*
K_1	*0.490747*	*0.508424*	*0.516452*
K_2	*2.824526*	*2.952272*	*2.945144*
$\sum\Lambda K_1$	*0.559845*	*0.545065*	*0.550420*
$\sum\Lambda K_2$	*3.222226*	*3.165037*	*3.138854*

Table 2. Solutions 1–3 are three sets of coefficients obtained from three independent constrained optimization processes by using the cubic spline scaling function.

V. Reconstructing Original Image from $\phi(x)$ and $\gamma(x)$

It has been mentioned in Section II that an image can possibly be reconstructed once the scaling function, the wavelet function as well as its corresponding dual wavelet are determined. In what follows, we will divide the whole reconstruction process into two parts. In the first part, the known functions $\phi(x)$ and $\gamma(x)$ will be used to derive their corresponding dual wavelet, $\xi(x)$. This part will be conducted in 1–D.

However, since an image is 2–D by nature, the derivation has to be extended to 2–D. Therefore, in the second part, the continuous functions $\phi(x)$, $\gamma(x)$ and $\xi(x)$ will first be converted into their 1–D discrete WTs. Then, the inverse WTs of theses discrete WTs are derived. The discrete WTs of $\phi(x)$, $\gamma(x)$ and $\xi(x)$ and their inverse in 1–D are then used to derive the 2–D format . Finally, an example describing how to apply the derived 2–D edge filter to detect edge points in arbitrary direction at different scales will be illustrated. It is based on these edge information an image can be reconstructed.

A. Deriving the Dual Wavelet $\xi(x)$

Based on Equations (12) and (14), the definitions of $\phi(x)$, $\gamma(x)$ and $\xi(x)$ in the frequency domain are clearly defined. Besides, their relationship is defined by Equation (15). In Section IV, we have chosen the quadratic spline function as the scaling function for deriving the desired edge filter. Therefore, $H(\omega)$ in Equation (12) is determined beforehand. Furthermore, based on a constrained optimization process, the set of coefficients for the desired wavelet can be decided. In other words, $G(\omega)$ in Equation (13) can be determined. Under the circumstances, $K(\omega)$ in Equation (14) can be obtained by solving Equation (15). Once $K(\omega)$ is determined, it can be plugged back into Equation (14) and then the dual wavelet $\xi(x)$ can be derived by taking the inverse Fourier transform of Equation (14). In what follows, the detailed procedure will be elaborated.

Based on Equation (32), the Fourier transform of a quadratic spline function has the following form:

$$\hat{\phi}(\omega) = \left[\frac{\sin \omega/2}{\omega/2}\right]^3. \tag{38}$$

From Equation (12) , if β_1 is set to 0, we obtain

$$H(\omega) = (\cos \omega/2)^3. \tag{39}$$

From the inverse Fourier transform, the set of $\{h(n)\}_{|n|\le 6}$ is shown in Table 3. It is easy to find that $h(n)$ is symmetric with respect to the origin. As to the desired wavelet $\gamma(x)$, if we let j=1, based on Equation (36), we have

$$\frac{1}{2}\gamma(\frac{x}{2}) = \sum_{n=0}^{M} c(n)[\phi(x + n + \frac{1}{2}) - \phi(x - n - \frac{1}{2})],$$

where M is a positive integer. Under the circumstances, the number of coefficients needed in an expansion is $2M+1$. In the subsequent derivation, M is consistently set to 5. By taking the Fourier transform, we have

$$\hat{\gamma}(2\omega) = i\sum_{n=0}^{M} 2c(n)\sin[(n+\frac{1}{2})\omega]\hat{\phi}(\omega). \tag{40}$$

It has been stated in Section IV that the best edge filter always appears when the shift is set to 1/2, i.e., $\hat{\gamma}(2\omega) = e^{-\frac{\omega}{2}}G(\omega)\hat{\phi}(\omega)$. From Equation (13), $G(\omega)$ can be derived

$$G(\omega) = ie^{i\frac{\omega}{2}}\sum_{n=0}^{M} 2c(n)\sin[(n+\frac{1}{2})\omega]. \tag{41}$$

n	$h(n)$	$g(n)$	$k(n)$	$l(n)$
–6	0.0	0.0	0.00000268	0.0
–5	–0.000423989	0.0	0.00166352	0.0
–4	0.00110237	0.0	–0.00519218	0.0
–3	–0.00404203	–0.092042	0.00721728	0.0078125
–2	0.0363783	–0.337216	–0.04377623	0.046875
–1	0.254648	–1.212978	0.20687030	0.1171875
0	0.424413	–1.915714	–0.20687030	0.65625
1	0.254648	1.915714	0.04377623	0.1171875
2	0.0363783	1.212978	–0.00721728	0.046875
3	0.0363783	0.337216	0.00519218	0.0078125
4	0.00110237	0.092042	–0.00166352	0.0
5	–0.000423989	0.0	–0.00000268	0.0

Table 3. Coefficients of the impulse response of the filters *h(n), g(n), k(n)* and *l(n)*.

The coefficient set of $\{g(n)\}_{|n|\le 6}$ can then be determined and is listed in Table 3. It is obvious that $\{g(n)\}$ is anti–symmetric with respect to 1/2. Finally, from Equation (15), $K(\omega)$ can be calculated as follows:

$$K(\omega) = \frac{e^{-i\frac{\omega}{2}}(1-\cos^6\omega/2)}{i\sum_{n=0}^{M} 2c(n)\sin[(n+\frac{1}{2})\omega]}. \tag{42}$$

The coefficients of $\{k(n)\}_{|n|\le 6}$ are listed in Table 3. Once $\{h(n)\}$, $\{g(n)\}$ and $\{k(n)\}$ are determined, the corresponding dual wavelet $\hat{\xi}(\omega)$ can be determined, where

$$\hat{\xi}(\omega) = e^{i\frac{\omega}{4}}K(\frac{\omega}{2})\hat{\phi}(\frac{\omega}{2}) = \frac{1-\cos^6\omega/4}{i\sum_{n=0}^{M} 2c(n)\sin[(\frac{n}{2}+\frac{1}{4})\omega]}\left[\frac{\sin\omega/4}{\omega/4}\right]^3. \tag{43}$$

Based the above results, the corresponding discrete WTs and their inverse as well can be calculated.

B. Deriving the Discrete WT and Inverse WT

In what follows, the derivation process is similar to Mallat–Zhong's method[4]. Let $h_{2^j}(n)$ and $g_{2^j}(n)$ denote the discrete filters obtained by putting $2^j - 1$ zeros between all two consecutive

coefficients of *h(n)* and *g(n),* respectively. Based on Equations (2) and (8), the discrete WT is given as follows:

$$S_{2^{j+1}}f(n) = S_{2^j}f * h_{2^j}(n), \tag{44}$$

and

$$W_{2^{j+1}}f(n) = S_{2^j}f * g_{2^j}(n). \tag{45}$$

Furthermore, by putting $\left\{W_{2^j}f(n)\right\}_{j>0}$ and $\left\{S_{2^j}f(n)\right\}_{j>0}$ back together the original image *f(x)* can be recovered. The process is the so–called inverse wavelet transform[4]. Based on Equation (9), the inverse WT is given as follows:

$$S_{2^{j-1}}f(n) = S_{2^j}f(n) * h_{2^{j-1}}(-n) + W_{2^j}f(n) * k_{2^{j-1}}(n), \tag{46}$$

where $k_{2^j}(n)$ is obtained by putting $2^j - 1$ zeros between all two consecutive coefficients of *k(n).*

Now, we illustrate the 2–D WT and its inverse WT. Let $\Phi(x, y)$ denote the scaling function as follows:

$$\Phi(x, y) = \phi(x)\phi(y),$$

whose Fourier transform is given by

$$\hat{\Phi}(\omega_x, \omega_y) = \hat{\phi}(\omega_x)\hat{\phi}(\omega_y) \quad \text{with} \quad \hat{\phi}(\omega) = e^{-i\beta_1\omega}\prod_{p=1}^{\infty} H(2^{-p}\omega), \tag{47}$$

where β_1 is a shift. In 2–D wavelet transform, there are two wavelets needed to be defined. Let $\gamma^1(x, y)$ and $\gamma^2(x, y)$ denote two wavelets in x and y directions, respectively, and $\xi^1(x, y)$ and $\xi^2(x, y)$ are their corresponding ''dual'' wavelets. Their Fourier transforms are as follows[4]:

$$\hat{\gamma}^1(2\omega_x, 2\omega_y) = e^{-i\beta_2\omega_x}G(\omega_x)\hat{\phi}(\omega_x)\hat{\phi}(\omega_y), \tag{48}$$

$$\hat{\gamma}^2(2\omega_x, 2\omega_y) = e^{-i\beta_2\omega_y}G(\omega_y)\hat{\phi}(\omega_x)\hat{\phi}(\omega_y), \tag{49}$$

$$\hat{\xi}^1(2\omega_x, 2\omega_y) = e^{i\beta_2\omega_x}K(\omega_x)L(\omega_y)\hat{\phi}(\omega_x)\hat{\phi}(\omega_y), \text{ and} \tag{50}$$

$$\hat{\xi}^2(2\omega_x, 2\omega_y) = e^{i\beta_2\omega_y}L(\omega_x)K(\omega_y)\hat{\phi}(\omega_x)\hat{\phi}(\omega_y), \tag{51}$$

where β_2 is another shift. The 2π periodic functions $G(\omega)$, $K(\omega)$ and $L(\omega)$ satisfy the following relations:

$$|H(\omega)|^2 + G(\omega)K(\omega) = 1, \text{ and } L(\omega) = \frac{1 + |H(\omega)|^2}{2}. \tag{52}$$

At scale 2^j, the 2–D wavelet transform of the function *f(x,y)* has two components defined respectively as follows:

$$W^1_{2^j}f(x, y) = f * \gamma^1_{2^j}(x, y) \text{ and } W^2_{2^j}f(x, y) = f * \gamma^2_{2^j}(x, y), \tag{53}$$

where $\gamma^1_{2^j}(x,y) = \frac{1}{2^{2j}}\gamma^1(\frac{x}{2^j},\frac{y}{2^j})$ and $\gamma^2_{2^j}(x,y) = \frac{1}{2^{2j}}\gamma^2(\frac{x}{2^j},\frac{y}{2^j})$. Besides, the 2–D smoothing operator S_{2^j} is defined as the convolution between *f(x,y)* and $\Phi_{2^j}(x,y)$, i.e.,

$$S_{2^j}f(x,y) = f * \Phi_{2^j}(x,y), \tag{54}$$

where $\Phi_{2^j}(x,y) = \frac{1}{2^{2j}}\Phi(\frac{x}{2^j},\frac{y}{2^j})$. Assume that *l(n)* is the inverse Fourier transform of $L(\omega)$. Let $l_{2^j}(n)$ denote the discrete filter obtained by putting $2^j - 1$ zeros between all two consecutive coefficients of *l(n),* and *d(n)* be the Dirac filter whose impulse response is equal to 1 at *n*=0 and 0 otherwise. We denote $S_{2^0}f$ as the finest resolution view and $S_{2^J}f$ the coarsest resolution view of *f(x,y)*. Based on Equations (53) and (54), a procedure which can be used to derive the 2–D discrete wavelet transform of *f(x,y)* has been proposed by Mallat and Zhong[4]. The procedure is described as follows:

$S_{2^0}f(x,y) = f(x,y)$; *j*=0;
while $j < J$ *do*
$W^1_{2^{j+1}}f(m,n) = S_{2^j}f(m,n) * [g_{2^j}(m), d(n)]$;
$W^2_{2^{j+1}}f(m,n) = S_{2^j}f(m,n) * [d(n), g_{2^j}(n)]$;
$S_{2^{j+1}}f(m,n) = S_{2^j}f(m,n) * [h_{2^j}(n), h_{2^j}(n)]$;
j=j+1;
end;

Here, $I(m,n) * [a(m), b(n)]$ specifies two separate sets of convolutions with respect to *m*, *n*, respectively, of an image *I(m,n)* using the 1–D filters *a(m)* and *b(n)*. As to the inverse WT, when a 1–D WT is extended into a 2–D WT, the format of Equation (9) can be rewritten as follows [4]:

$$S_{2^{j-1}}f(x,y) * \overline{\Phi}_{2^{j-1}}(x,y) - S_{2^j}f(x,y) * \overline{\Phi}_{2^j}(x,y) = W^1_{2^j}f(x,y) * \xi^1_{2^j}(x,y) + W^2_{2^j}f(x,y) * \xi^2_{2^j}(x,y), \tag{55}$$

where $\overline{\Phi}(x,y) = \Phi(-x,-y)$, $\xi^1_{2^j}(x,y) = \frac{1}{2^{2j}}\xi^1(\frac{x}{2^j},\frac{y}{2^j})$ and $\xi^2_{2^j}(x,y) = \frac{1}{2^{2j}}\xi^2(\frac{x}{2^j},\frac{y}{2^j})$. Based on Equation (55), Mallat and Zhong[4] proposed a procedure for deriving the discrete inverse 2–D wavelet transform of *f(x,y)* as follows:

j=J;
while $j > 0$ *do*
$S_{2^{j-1}}f(m,n) = S_{2^j}f(m,n) * [h_{2^{j-1}}(-m), h_{2^{j-1}}(-n)] + W^1_{2^j}f(m,n) * [k_{2^{j-1}}(m), l_{2^{j-1}}(n)]$

$$+ \; W^2_{2^j} f(m,n) * [l_{2^{j-1}}(m), k_{2^{j-1}}(n)];$$

j=j–1;

end.

Based on the above information, it is sufficient to reconstruct the original image.

Next, we will illustrate how to use $W^1_{2^j} f(x,y)$ and $W^2_{2^j} f(x,y)$ to calculate some related information of the detected edge points from an image. At scale 2^j, the modulus of the gradient vector of the input image *f(x,y)* is defined as follows [4]:

$$M_{2^j} f(x,y) = \sqrt{|W^1_{2^j} f(x,y)|^2 + |W^2_{2^j} f(x,y)|^2}, \tag{56}$$

and the degree of the gradient vector is:

$$A_{2^j} f(x,y) = Arg(W^1_{2^j} f(x,y) + i \; W^2_{2^j} f(x,y)). \tag{57}$$

If we locate the point, whose modulus has a local maxima and is larger than a threshold, then it is classified as an edge point. Thus, the edge points at scale 2^j in any direction can be exactly detected. At the corresponding locations, by using the magnitudes of $M_{2^j} f(x,y)$, the edge strengths can be determined. Furthermore, based on the values of $A_{2^j} f(x,y)$, the directions of the detected edges are decided. The above procedure is the so–called multi–scale edge detection [4].

VI. Experimental Results

A series of experiments have been conducted to corroborate the proposed theory. Three standard 256×256 images, Lena (Figure 1.(a)), house (Figure 1.(b)) and multi–pepper (Figure 1.(c)), were adopted to test the effectiveness of the proposed edge filter. In the experiments, the format of the wavelet adopted was as follows (Equation (36)):

$$\gamma(x) = \frac{1}{4} \sum_{n=0}^{5} c(n)[\phi(\frac{x}{4} + n + \frac{1}{2}) - \phi(\frac{x}{4} - n - \frac{1}{2})].$$

When this wavelet was extended to the 2–D case, there would be two wavelets in x and y directions, respectively. They were:

$$\gamma^1(x,y) = \gamma(x)\frac{1}{4}\phi(\frac{y}{4}) \qquad \text{and} \qquad \gamma^2(x,y) = \frac{1}{4}\phi(\frac{x}{4})\gamma(y).$$

In the real implementation, the convolution between an image $f(x,y)$ and $\gamma^1(x,y)$ was first performed in x direction, then followed by the convolution with $\frac{1}{4}\phi(\frac{x}{4})$ in y direction. In this way, the partial derivative of

$f(x,y)$ in x direction, f_x, could be obtained. Similarly, the partial derivative of f in y direction, f_y, was obtained by convoluting $f(x,y)$ with $\gamma(y)$ in y direction followed by another convolution with $\frac{1}{4}\phi(\frac{x}{4})$ in x direction. The gradient vector (f_x, f_y) provided the rate of change of intensity at a point (x,y). If we locate the local maximum of $M(x,y) = \sqrt{f_x^2 + f_y^2}$ and threshold it, all the edge points of $f(x,y)$ can be detected. Here, a threshold T was used to delete the spurious edge points [3], [4]. In all experiments, the T was set to 25 for all images. Before thresholding, the value of edge strength of each point was normalized such that its value ranged from 0 to 255. In order for comparison, the Mallat–Zhong's approach was also implemented and tested on the set of images. Figure 2(a), (c), and (e) show a series of results when Mallat–Zhong's wavelet was applied to the Lena image at different scales. In contrast to the above results, Figure 2(b), (d), and (f) show the corresponding results which were obtained by applying our filter. Figures 3 and 4 show the results of another two series of experiments on the house image and the multi–pepper image, respectively. One thing to be noticed is that there were no preprocessing or postprocessing involved in the whole procedure. From the above results, it is obvious that our results contained less noise information than those obtained by Mallat–Zhong's method. For example, in Figure 2(a) there exists many noises as well as discontinuities near the pillar and the hat of the Lena image. However, these defects did not happen in our result (Figure 2(b)). The above fact means our method has better ability to remove noises and to preserve edge continuity in an image. From the resolution viewpoint, both Mallat–Zhong's wavelet and ours behaved similarly. That is, a coarse resolution resulted in fewer spurious responses as well as better effect on noise removal. However, low resolution also lose the precision of edge localization. In our experiments, when the resolution S was set to 2^2, the performance was the best in terms of noise removal and precision. On the other hand, from the detected edge information $\left\{W_{2^j}^1 f(m,n)\right\}_{j=1,2,3}$ and $\left\{W_{2^j}^2 f(m,n)\right\}_{j=1,2,3}$ as well as the coarsest view $S_{2^3} f(m,n)$, the original image $f(x,y)$ can be reconstructed approximately by using the inverse wavelet transform. Figure 5 (a), (b) and (c) show the reconstruction results of the Lena, the house and the multi–pepper images, respectively. From the reconstructed images, it is hard to distinguish the differences between the original images and the reconstructed ones.

VII.Conclusions and Discussions

In this report, we have proposed a new wavelet–based approach to solving the edge detection problem. This scheme has taken advantage of the properties of wavelet transform and Canny's criteria to derive a wavelet such that the edge points can be detected efficiently and accurately. The proposed edge filter is

similar to a gradient filter. Since it is wavelet–based, the inherent multiresolution nature of a wavelet provides more flexibility in the analysis of images. Unlike Mallat–Zhong's filter, the proposed edge filter was derived by executing an optimization process. Therefore, the performance of the proposed filter is much better than that of Mallat–Zhong's edge detector. In real implementation, the proposed filter is easy to implement.

In comparison with Mallat–Zhong's wavelet–based approach[4], our method is different in several aspects. First, although Mallat–Zhong's method was able to detect edges at different scales, its ultimate goal was to reconstruct the whole image from the pieces of edge maps which were extracted from different scales. The first derivative of a cubic spline function was chosen as their mother wavelet. The capability of their edge filter is limited. In this report, the desired wavelet was derived by executing an optimization process. This process tried to optimize three criteria proposed by Canny. Under the circumstances, it is obvious that our filter certainly produced better results than that of Mallat–Zhong's. From the experimental results, it is apparent that our results contained less noise information than those obtained by Mallat–Zhong's method.

APPENDIX

In this appendix, the calculation of several integrals and derivatives which are needed in the determination of $\Sigma(\gamma)$, $\Lambda(\gamma')$ and $K(\gamma)$ will be elaborated as follows:

Case 1: The derivation of $\int_{-\infty}^{0} \gamma(x)$.

$$\int_{-\infty}^{0} \gamma(x) = \sum_{n=0}^{N} 2c(n) \int_{-\infty}^{0} [\phi(2x + n + \alpha) - \phi(2x - n - \alpha)]dx = \sum_{n=0}^{N} c(n) \int_{-n-\alpha}^{n+\alpha} \phi(y)dy.$$

Let $R_1 = \int_{-n-\alpha}^{n+\alpha} \phi(y)dy$. Plugging $\phi^3(x)$ into R_1, the following cases have to be considered:

when $0 \le \alpha \le 1/2$,

$$R_1 = \begin{cases} 3\alpha/4 - \alpha^3/3, & \text{if } n = 0, \\ 23/48 + \alpha/8 - \alpha^2/4 + \alpha^3/6, & \text{if } n = 1, \\ 1/2, & \textit{otherwise}; \end{cases}$$

when $1/2 < \alpha < 1$,

$$R_1 = \begin{cases} -1/16 + 9\alpha/8 - 3\alpha^2/4 + \alpha^3/6, & \text{if } n = 0, \\ 1/2, & \textit{otherwise}\ . \end{cases}$$

Case 2: The derivation of $\int_{-\infty}^{\infty} \gamma^2(x)$.

$$\int_{-\infty}^{\infty} \gamma^2(x) = \sum_{m=0}^{N} \sum_{n=0}^{N} 4c(m)c(n) \int_{-\infty}^{\infty} [\phi(2x + m + \alpha) - \phi(2x - m - \alpha)][\phi(2x + n + \alpha) - \phi(2x - n - \alpha)]dx,$$

$$= \sum_{m=0}^{N} \sum_{n=0}^{N} 4c(m)c(n) \int_{-\infty}^{\infty} [\phi(x)\phi(x + m - n) - \phi(x)\phi(x + m + n + 2\alpha)]dx.$$

Let $R_2 = \int_{-\infty}^{\infty} \phi(x)\phi(x + m - n)dx$, and $T_2 = \int_{-\infty}^{\infty} \phi(x)\phi(x + m + n + 2\alpha)dx$. Plugging $\phi^3(x)$ into R_2 and T_2, we have

$$R_2 = \begin{cases} 11/20, & \text{if } \ m - n = 0, \\ 13/60, & \text{if } \ m - n = \pm\ 1, \\ 1/120, & \text{if } \ m - n = \pm\ 2, \\ 0, & \textit{otherwise}\ . \end{cases}$$

For the case of T_2, the following conditions have to be considered. If $0 \le \alpha \le 1/2$,

$$T_2 = \begin{cases} 11/20 - 2\alpha^2 + 4\alpha^4 - 8\alpha^5/3, & \text{if } m+n=0, \\ 13/60 - 5\alpha/6 + 2\alpha^2/3 + 4\alpha^3/3 - 8\alpha^4/3 + 4\alpha^5/3, & \text{if } m+n=1, \\ 1/120 - \alpha/12 + \alpha^2/3 - 2\alpha^3/3 + 2\alpha^4/3 - 4\alpha^5/15, & \text{if } m+n=2, \\ 0, \ \textit{otherwise}; \end{cases}$$

and if $1/2 < \alpha < 1$,

$$T_2 = \begin{cases} 17/40 + 5\alpha/4 - 7\alpha^2 + 10\alpha^3 - 6\alpha^4 + 4\alpha^5/3, & \text{if } m+n=0, \\ 4/15 - 4\alpha/3 + 8\alpha^2/3 - 8\alpha^3/3 + 4\alpha^4/3 - 4\alpha^5/15, & \text{if } m+n=1, \\ 0, & \textit{otherwise}. \end{cases}$$

Case 3: The derivation of $\int_{-\infty}^{\infty} \gamma'^2(x)$.

$$\int_{-\infty}^{\infty} \gamma'^2(x) = 16 \sum_{m=0}^{N} \sum_{n=0}^{N} c(m)c(n) \int_{-\infty}^{\infty} [\phi'(x)\phi'(x+m-n) - \phi'(x)\phi'(x+m+n+2\alpha)]dx.$$

Let $R_3 = \int_{-\infty}^{\infty} \phi'(x)\phi'(x+m-n)dx$, and $T_3 = \int_{-\infty}^{\infty} \phi'(x)\phi'(x+m+n+2\alpha)dx$. Plugging $\phi^3(x)$ into R_3 and T_3, we have

$$R_3 = \begin{cases} 1, & \text{if } m-n=0, \\ -1/3, & \text{if } m-n=\pm 1, \\ -1/6, & \text{if } m-n=\pm 2, \\ 0, & \textit{otherwise}. \end{cases}$$

As to the case of T_3, the following situations have to be considered. If $0 \le \alpha \le 1/2$,

$$T_3 = \begin{cases} 1 - 12\alpha^2 + 40\alpha^3/3, & \text{if } m+n=0, \\ -1/3 - 2\alpha + 8\alpha^2 - 20\alpha^3/3, & \text{if } m+n=1, \\ -1/6 + \alpha - 2\alpha^2 + 4\alpha^3/3, & \text{if } m+n=2, \\ 0, & \textit{otherwise}; \end{cases}$$

and if $1/2 < \alpha < 1$,

$$T_3 = \begin{cases} 7/2 - 15\alpha + 18\alpha^2 - 20\alpha^3/3, & \text{if } m+n=0, \\ -4/3 + 4\alpha - 4\alpha^2 + 4\alpha^3/3, & \text{if } m+n=1, \\ 0, & \textit{otherwise}. \end{cases}$$

Case 4: The derivation of .

$|\gamma'(0)| = |\sum_{n=0}^{N} 2c(n) \int_{-\infty}^{\infty} [\phi'(2x+n+\alpha) - \phi'(2x-n-\alpha)]dx|$. If $0 \le \alpha \le 1/2$, $|\gamma'(0)| = -16\alpha\, c(0) + (8\alpha - 4)c(1)$; and if $1/2 < \alpha < 1$, $|\gamma'(0)| = (8\alpha - 12)c(0)$.

Case 5: The derivation of $\int_{-\infty}^{\infty} \gamma''^2(x)$.

$$\int_{-\infty}^{\infty} \gamma''^2(x) = 64 \sum_{m=0}^{N} \sum_{n=0}^{N} c(m)c(n) \int_{-\infty}^{\infty} [\phi''(x)\phi''(x+m-n) - \phi''(x)\phi''(x+m+n+2\alpha)]dx.$$

Let $R_4 = \int_{-\infty}^{\infty} \phi''(x)\phi''(x+m-n)dx$, and $T_4 = \int_{-\infty}^{\infty} \phi''(x)\phi''(x+m+n+2\alpha)dx$. Plugging $\phi^3(x)$ into R_4 and T_4, we have

$$R_4 = \begin{cases} 6, & \text{if } m-n=0, \\ -4, & \text{if } m-n=\pm 1, \\ 1, & \text{if } m-n=\pm 2, \\ 0, & \textit{otherwise}. \end{cases}$$

As to the case of T_4, the following situations have to be considered. If $0 \le \alpha \le 1/2$,

$$T_4 = \begin{cases} 6-20\alpha, & \text{if } m+n=0, \\ -4+10\alpha, & \text{if } m+n=1, \\ 1-2\alpha, & \text{if } m+n=2, \\ 0, & \textit{otherwise}, \end{cases}$$

and if $1/2 < \alpha < 1$,

$$T_4 = \begin{cases} -9+10\alpha, & \text{if } m+n=0, \\ 2-2\alpha, & \text{if } m+n=1, \\ 0, & \textit{otherwise}. \end{cases}$$

As to the multiple response criteria, if Sarkar–Boyer's criterion [9] is used, the following integral is needed.

Case 6: The derivation of $\int_{-\infty}^{\infty} x^2\gamma^2(x)$.

$$\int_{-\infty}^{\infty} x^2\gamma^2(x) = \sum_{m=0}^{N} \sum_{n=0}^{N} 4c(m)c(n) \int_{-\infty}^{\infty} x^2[\phi(2x+m+\alpha) - \phi(2x-m-\alpha)][\phi(2x+n+\alpha) - \phi(2x-n-\alpha)]dx$$

$$= \frac{1}{2} \sum_{m=0}^{N} \sum_{n=0}^{N} c(m)c(n) \left\{ \int_{-\infty}^{\infty} [(y-m-\alpha)^2 + (y+n+\alpha)^2]\phi(y)\phi(y+m-n)dy \right.$$
$$\left. - \int_{-\infty}^{\infty} [(y+m+\alpha)^2 + (y+n+\alpha)^2]\phi(y)\phi(y+m+n+2\alpha) \right\} dy.$$

Let $R_5 = \int_{-\infty}^{\infty} [(y-m-\alpha)^2 + (y+n+\alpha)^2]\phi(y)\phi(y+m-n)dy$, and $T_5 = \int_{-\infty}^{\infty} [(y+m+\alpha)^2 + (y+n+\alpha)^2]\phi(y)\phi(y+m+n+2\alpha)dy$. Plugging $\phi^3(x)$ into R_5 and T_5, we have

$$R_5 = \begin{cases} \frac{43}{280} + \frac{11\alpha^2}{10} + \frac{11\alpha n}{5} + \frac{11n^2}{10}, \text{ if } m - n = 0, \\ \frac{131}{840} + \frac{13\alpha}{30} + \frac{13\alpha^2}{30} + \frac{13n}{30} + \frac{13\alpha n}{15} + \frac{13n^2}{30}, \text{ if } m - n = 1, \\ \frac{131}{840} - \frac{13\alpha}{30} + \frac{13\alpha^2}{30} - \frac{13n}{30} + \frac{13\alpha n}{15} + \frac{13n^2}{30}, \text{ if } m - n = -1, \\ \frac{29}{1680} + \frac{\alpha}{30} + \frac{\alpha^2}{60} + \frac{n}{30} + \frac{\alpha n}{30} + \frac{n^2}{60}, \text{ if } m - n = 2, \\ \frac{29}{1680} - \frac{\alpha}{30} + \frac{\alpha^2}{60} - \frac{n}{30} + \frac{\alpha n}{30} + \frac{n^2}{60}, \text{ if } m - n = -2, \\ 0, \quad \textit{otherwise} . \end{cases}$$

As to T_5, we have to consider the following situations. If $0 \leq \alpha \leq 1/2$,

$$T_5 = \begin{cases} \frac{43}{280} - \frac{7\alpha^2}{10} + 2\alpha^4 - \frac{12\alpha^5}{5} + \frac{8\alpha^6}{5} - \frac{16\alpha^7}{21} + \\ \qquad \frac{11n^2}{10} - 4\alpha^2 n^2 + 8\alpha^4 n^2 - \frac{16\alpha^5 n^2}{3}, \text{ if } m + n = 0, \\ \frac{131}{840} - \frac{13\alpha}{20} + \frac{19\alpha^2}{30} + \alpha^3 - \frac{8\alpha^4}{3} + \frac{34\alpha^5}{15} - \frac{16\alpha^6}{15} + \frac{8\alpha^7}{21} + \\ \qquad (\frac{13}{30} - \frac{5\alpha}{3} + \frac{4\alpha^2}{3} + \frac{8\alpha^3}{3} - \frac{16\alpha^4}{3} - \frac{8\alpha^5}{3}) \times (n^2 - n), \text{ if } m + n = 1, \\ \frac{29}{1680} - \frac{7\alpha}{40} + \frac{43\alpha^2}{60} - \frac{3\alpha^3}{2} + \frac{5\alpha^4}{3} - \frac{14\alpha^5}{15} + \frac{4\alpha^6}{15} - \frac{8\alpha^7}{105} + \\ \qquad (\frac{1}{60} - \frac{\alpha}{6} + \frac{2\alpha^2}{3} - \frac{4\alpha^3}{3} + \frac{4\alpha^4}{3} - \frac{8\alpha^5}{15}) \times (n^2 - 2n), \text{ if } m + n = 2, \\ 0, \ \textit{otherwise}; \end{cases}$$

and if $1/2 < \alpha < 1$,

$$T_5 = \begin{cases} \frac{5}{112} + \frac{9\alpha}{8} - \frac{109\alpha^2}{20} + \frac{21\alpha^3}{2} - 11\alpha^4 + \frac{34\alpha^5}{5} - \frac{12\alpha^6}{5} + \frac{8\alpha^7}{21}, \text{ if } m + n = 0, \\ \frac{22}{105} - \frac{6\alpha}{5} + \frac{44\alpha^2}{15} - 44\alpha^3 + \frac{10\alpha^4}{3} - \frac{26\alpha^5}{15} + \frac{8\alpha^6}{15} - \frac{8\alpha^7}{105} + \\ \qquad (\frac{8}{15} - \frac{8\alpha}{3} + \frac{16\alpha^2}{3} - \frac{16\alpha^3}{3} + \frac{8\alpha^4}{3} - \frac{8\alpha^5}{15}) \times (n^2 - n), \text{ if } m + n = 1, \\ 0, \ \textit{otherwise} . \end{cases}$$

REFERENCES

[1] D. Marr and E. Hildreth, ''Theory of edge detection,'' Proc. *Royal Soc. London B,* vol. 207, pp.187–217, 1980.

[2] R. M. Haralick, ''Digital step edges from zero crossing of second directional derivatives,'' *IEEE Trans. Pattern Anal. Machine Intell*., vol. PAMI–6, no. 1, pp. 58–68, Jan. 1984.

[3] J. F. Canny, ''A computational approach to edge detection,'' *IEEE Trans. Pattern Anal. Machine Intell*., vol. PAMI–8, no. 6, pp. 679–697, Nov. 1986.

[4] S. Mallat and S. Zhong, ''Characterization of signals from multi–scale edges,'' *IEEE Trans. Pattern Anal. Machine Intell*., vol. PAMI–14, no. 7, pp. 710–732, July 1992.

[5] M. Sun, R. J. Sclabassl, C. C. Li, Y. Zhang and Harold Szu, ''Symmetrical wavelet transforms for edge localization,'' *Optical Engineering*, vol. 33, no. 7, pp. 2272–2281, July 1994.

[6] D. J. Williams, and M. Shah, ''Edge contours using multiple scales,'' *Comput. Vision Graphics Image Processing*, vol. 51, pp. 256–274, 1990.

[7] V. Torre and T. Poggio, ''On edge detection,'' *IEEE Trans. Pattern Anal. Machine Intell*., vol PAMI–8, no. 2, pp. 147–163, March 1986.

[8] V. Yuille and T. Poggio, ''Scaling theorems for zero crossings,'' *IEEE Trans. Pattern Anal. Machine Intell*., vol PAMI–8, pp. 15–25, Jan. 1986.

[9] S. Sarkar and K. L. Boyer , ''On optimal infinite impulse response edge detection filters,'' *IEEE Trans. Pattern Anal. Machine Intell*., vol. PAMI–13, no. 11, pp. 1154–1171, Nov. 1991.

[10] I. E. Sobel, *Camera Models and Machine Perception*, Ph.D. thesis, Standford University, 1970.

[11] D. Geman, S. Geman, C. Graffigne, and P. Dong, ''Boundary detection by constrained optimization,'' *IEEE Trans. Pattern Anal. Machine Intell*., vol. PAMI–12, no. 7, pp. 609–628, July. 1990.

[12] R. Deriche, ''Using Canny's criteria to derive a recusively implemented optimal edge detector,'' *Int. J. Computer Vision*, pp.167–187, 1987.

[13] H. Heuckel, ''An operator which locates edges in digitized pictures.'' *J. Assoc. Comput. Machine.*, vol. 18, pp.113–115, Jan. 1971.

[14] H. Heuckel, ‘‘A local visual operator which recognizes edges and linear local numerical processing .’’ *J. Assoc. Comput. Machine.*, vol. 20, pp. 634–647, Oct. 1973.

[15] K. S. Shanmugam, F. M. Dickey, and J. A. Green, ‘‘An optimal frequency domain filter for edge detection in digital pictures,’’ *IEEE Trans. Pattern Anal. Machine Intell.*, vol. PAMI–1, no. 1, pp. 37–49, Jan. 1979.

[16] W. H. H. F. Lunscher, ‘‘The asymptotic optimal frequency domain filter for edge detection, ’’ *IEEE Trans. Pattern Anal. Machine Intell.*, vol. PAMI–5, no. 6, pp. 678–680, Nov. 1983.

[17] W. H. H. F. Lunscher and M. P. Beddoes, ‘‘Optimal edge detector design I: parameter selection and noise effects,’’ *IEEE Trans. Pattern Anal. Machine Intell.*, vol. PAMI–8, no. 2, pp. 164–177, March 1986.

[18] W. H. H. F. Lunscher and M. P. Beddoes, ‘‘Optimal edge detector design II: coefficient quantization,’’ *IEEE Trans. Pattern Anal. Machine Intell.*, vol. PAMI–8, no. 2, pp. 178–187, March 1986.

[19] N. E. Nahi and M. H. Jahanshi, ‘‘Image boundary estimation,’’ *IEEE Trans. Comput.*, vol. C–26, pp. 772–781, Aug. 1977.

[20] J. S. Huang and D. H. Tseng, ‘‘Statistical theory of edge detection,’’ *Comput. Vision Graphics Image Processing*, vol. 43, pp. 337–346, 1988.

[21] Jun Shen and Serge Castan, ‘‘An optimal linear operator for step edge detection,’’ *Comput. Vision Graphics Image Processing*, vol. 54, no. 2, pp. 112–133, March 1992.

[22] H. Y. Liao, M. Middler, and W. C. Lin, ‘‘Neural networks for step edge detection,’’ *Proc. International Joint Conf. on Neural Networks* II, Seattle, pp. 936, 1991.

[23] H. Y. Liao and M. Middler, ‘‘Neural networks for step edge detection using simulated annealing technique,’’ *Journal of Information Science and Engineering*, vol. 8, pp. 207–222, 1992.

[24] A. Cohen, I. Daubechies and J. C. Feauveau, ‘‘Bi–orthognal bases of compactly supported wavelets,’’ *Comm. Pure and Appl. Math.,* vol. PAMI–14, pp. 485–560, 1992.

[25] S. Mallat, ‘‘Mutifrequency channel decompositions of images and wavelet models,’’ *IEEE Trans. Acoustics, Speech, Signal Processing*, vol. ASSP–37, no. 12, pp. 2091–2110, Dec. 1989.

[26] S. Mallat, ‘‘A theory for multiresolution signal decomposition: The wavelet representation,’’ *IEEE Trans. Pattern Anal. Machine Intell.*, vol. PAMI–11, no. 12, pp. 674–693, July 1989.

[27] S. Mallat, ‘‘Multiresolution approximation and wavelet orthonormal bases of $L(R^2)$,’’ *Trans. Amer. Math. Soc.*, vol. 3–15, pp. 69–87, Sept. 1989.

[28] I. Daubechies, ‘‘The wavelet transform, time–frequency localization and signal analysis,’’ *IEEE Trans. Information Theory.*, vol. 36, no. 5, pp. 961–1005, Sept. 1990.

[29] C. K. Chui, (ed.), *Wavelet: A Tutorial in Theory and Applications*, Academic Press, New York, 1992.

[30] V. Perrier, ‘‘Towards a method for solving partial differential equations using wavelet bases,’’ *Wavelets: time–frequency methods and phase space* ed. by J. M. Combes, A. Grossman and Ph. Tchamithian, Sprinber–Verlag, pp. 269–283, 1989.

[31] J. S. Lienard and C. d’ Alssandro, ‘‘Wavelets and Granular analysis of speech,’’ *Wavelets: time–frequency methods and phase space* ed. by J. M. Combes, A. Grossman and Ph. Tchamithian, Sprinber–Verlag, pp. 158–163, 1989.

[32] S. O. Rice, ‘‘Mathematical analysis of random noise,’’ *Bell Syst. Tech. J.*, vol. 24, pp. 44–156, 1945.

[33] Y. Sheng, D. Roberge, Harold Szu, and T. Lu, ‘‘Optical wavelet matched filters for shift–invariant pattern recognition,’’ *Optics Letters*, vol. 18, no. 4, pp. 299–301, Feb. 1993.

[34] J. W. Hsieh, H. Y. Liao, and K. C. Fan, ‘‘A new approach for edge detection using wavelet transforms,’’ *Proc. Asian Conf. on Computer Vision*, Osaka, Japan, pp. 520–525, Nov. 1993.

(a) Lena image.

(b) House image

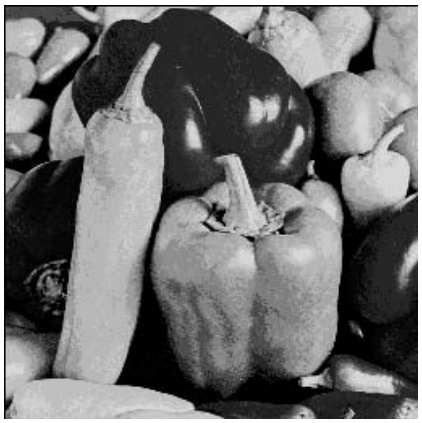

(c) Multi–pepper image

Fig. 1. (a)–(c) show a series of original images: (a) the Lena image, (b) the house image, and (c) the multi–pepper image.

(a) Edge points from $W_{2^1}^1 f(m,n)$ and $W_{2^1}^2 f(m,n)$ using Mallat′s wavelet .

(b) Edge points from $W_{2^1}^1 f(m,n)$ and $W_{2^1}^2 f(m,n)$ using our wavelet .

(c) Edge points from $W^1_{2^2}f(m,n)$ and $W^2_{2^2}f(m,n)$ using Mallat–Zhong's wavelet.

(d) Edge points from $W^1_{2^2}f(m,n)$ and $W^2_{2^2}f(m,n)$ using our method.

(e) Edge points from $W^1_{2^3}f(m,n)$ and $W^2_{2^3}f(m,n)$ using Mallat–Zhong's wavelet

(f) Edge points from $W^1_{2^3}f(m,n)$ and $W^2_{2^3}f(m,n)$ using our method.

Figure 2 (a), (c), and (e) represent respectively the detected edges when Mallat–Zhong's filter is applied to the Lena image at scale $S = 2^1$, 2^2, and 2^3. (b), (d) and (f) are the results obtained by applying our wavelet on the Lena image at $S = 2^1$, 2^2, and 2^3, respectively.

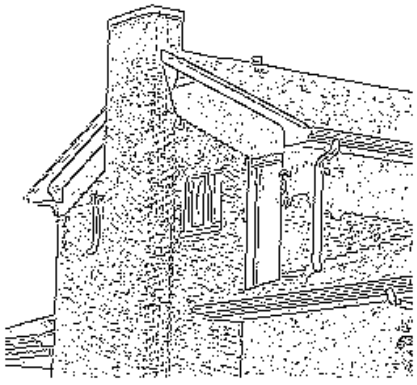

(a) Edge points from $W^1_{2^1}f(m,n)$ and $W^2_{2^1}f(m,n)$ using Mallat–Zhong's wavelet.

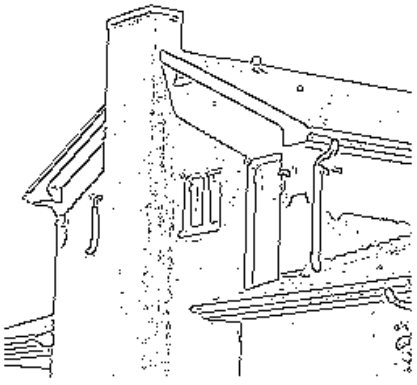

(b) Edge points from $W^1_{2^1}f(m,n)$ and $W^2_{2^1}f(m,n)$ using our method .

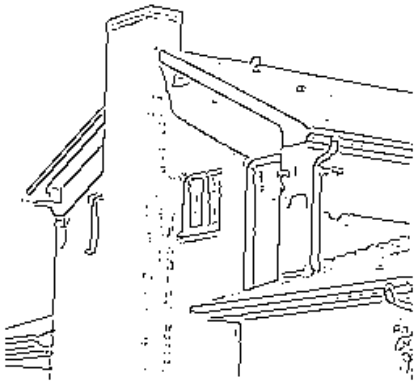

(c) Edge points from $W^1_{2^2}f(m,n)$ and $W^2_{2^2}f(m,n)$ using Mallat–Zhong's wavelet.

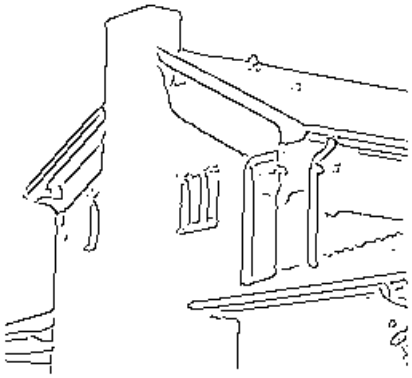

(d) Edge points from $W^1_{2^2}f(m,n)$ and $W^2_{2^2}f(m,n)$ using our method.

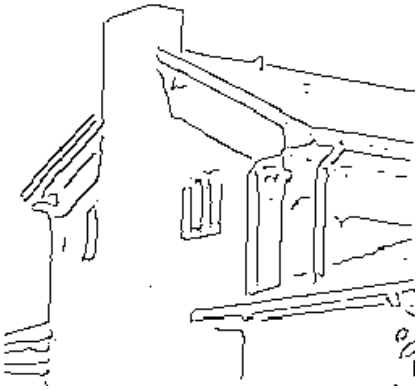

(e) Edge points from $W^1_{2^3}f(m,n)$ and $W^2_{2^3}f(m,n)$ using Mallat–Zhong's wavelet

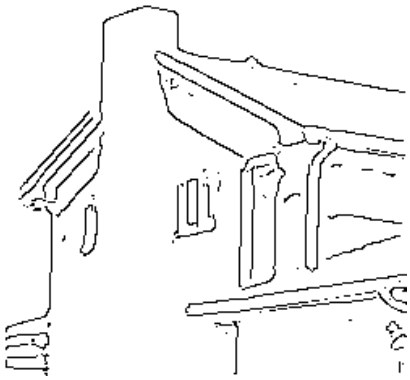

(f) Edge points from $W^1_{2^3}f(m,n)$ and $W^2_{2^3}f(m,n)$ using our method.

Figure 3 (a), (c), and (e) represent respectively the detected edges when Mallat–Zhong's filter is applied to the house image at scale $S = 2^1$, 2^2, and 2^3. (b), (d) and (f) are the results obtained by applying our wavelet on the house image at $S = 2^1$, 2^2, and 2^3, respectively.

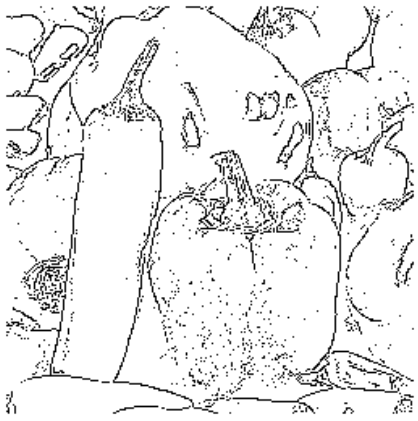

(a) Edge points from $W^1_{2^1}f(m,n)$ and $W^2_{2^1}f(m,n)$ using Mallat–Zhong's wavelet.

(b) Edge points from $W^1_{2^1}f(m,n)$ and $W^2_{2^1}f(m,n)$ using our method .

(c) Edge points from $W^1_{2^2}f(m,n)$ and $W^2_{2^2}f(m,n)$ using Mallat–Zhong's wavelet.

(d) Edge points from $W^1_{2^2}f(m,n)$ and $W^2_{2^2}f(m,n)$ using our method.

(e) Edge points from $W^1_{2^3}f(m,n)$ and $W^2_{2^3}f(m,n)$ using Mallat–Zhong's wavelet

(f) Edge points from $W^1_{2^3}f(m,n)$ and $W^2_{2^3}f(m,n)$ using our method.

Figure 4 (a), (c), and (e) represent respectively the detected edges when Mallat–Zhong's filter is applied to the multi–pepper image at scale $S = 2^1$, 2^2, and 2^3. (b), (d) and (f) are the results obtained by applying our wavelet on the multi–pepper image at $S = 2^1$, 2^2, and 2^3, respectively.

(a) Lena image.

(b) House image

(c) Multi–pepper image

Figure 5 Based on $\left\{W_{2^j}^1 f(m,n)\right\}_{j=1,2,3}$, $\left\{W_{2^j}^2 f(m,n)\right\}_{j=1,2,3}$ and the coarsest view $S_{2^3} f(m,n)$, the reconstructed Lena image, house image, and multi–pepper image are illustrated respectively in (a), (b) and (c).

In this paper, the wavelet theory is applied to solve the edge detection as well as the image reconstruction problems. By the above formulation, the problem becomes to determine the coefficients *h(n)*, $g(n)$ and $k(n)$ such that the edge points can be detected efficiently and the original image can be reconstructed correctly. Since the scaling function $\phi(x)$ will be chosen in advance and *h(n)*'s can be derived accordingly. Then, the major work is to derive the coefficients $g(n)$ and $k(n)$. In this paper, a constrained optimization process is used to guide the derivation of the coefficients set *g(n)*'s. In the optimization process, Canny's criteria are introduced as the constraints and the properties of wavelet theory are used. After that, the set of coefficients *k(n)*'s can be determined from the coefficients $h(n)$'s and $g(n)$'s. Thus, the dual wavelet is constructed. From the functions $\phi(x)$, $\psi(x)$ and $\xi(x)$, the so–called discrete wavelet transform and its corresponding inverse transform are developed for efficient data analysis.

VIII. Accuracy of Edge Localization Across Scales

In the previous section, in order to make the coefficients $\{g(n)\}_{n\in Z}$ decay quickly, an appropriate shift is made. This shift makes the set of coefficients *g(n)* be anti–symmetric with respect to $1/2$. It has been pointed out in [5] that this kind of adjustment will result in a displacement of the edge position between the input *f(n)* and the output $W_{2^j}f(n)$. The effect of delocalization is more significant when the scale j increases. This phenomenon also happens in Mallat–Zhong's approach [4], [5], [6]. In what follows, we will analyze the amount of shift and then propose a solution to this potential problem.

In Fourier theory, if a shift is made on β in the input signal *f(n),* then there exists a phase shift β in the Fourier transform of *f(n)*. Based on this understanding, the phase change of $W_{2^j}f(n)$ can be used to estimate the amount of edge displacement. Assume that the coefficient set *h(n)* of the low–pass filter is symmetric with respect to β_1 and that of the high–pass filter (*g(n)*) is anti–symmetric to β_2. Then, their Fourier transforms can be rewritten as follows:

$$H(\omega) = \overline{H}(\omega)e^{-i\beta_1\omega},$$

and

$$G(\omega) = \overline{G}(\omega)e^{-i\beta_2\omega},$$

where the inverse Fourier transform of $\overline{H}(\omega)$ and $\overline{G}(\omega)$ are symmetric and anti–symmetric with respect to the origin, respectively. Assume that *f(n)* has N points and $\omega_k = \frac{2\pi k}{N}$, k=0, 1, .., N–1. By taking the discrete Fourier transform of Equations (44) and (45) and applying recursively, we have

$$\hat{W}_{2^j}f(\omega_k) = \hat{S}_{2^{j-1}}f(\omega_k)\overline{G}(2^{j-1}\omega_k)e^{-i2^{j-1}\beta_2\omega_k},$$

$$= \hat{S}_{2^{j-2}} f(\omega_k)\overline{H}(2^{j-2}\omega_k)\overline{G}(2^{j-1}\omega_k)e^{-i2^{j-2}\beta_1\omega_k}e^{-i2^{j-1}\beta_2\omega_k},$$

$$= F(\omega_k)\left\{\prod_{n=0}^{j-2}\overline{H}(2^n\omega_k)\right\}\overline{G}(2^{j-1}\omega_k)e^{-i\beta_1\omega_k\sum_{n=0}^{j-2}2^n}e^{-i2^{j-1}\beta_2\omega_k},$$

$$= F(\omega_k)\left\{\prod_{n=0}^{j-2}\overline{H}(2^n\omega_k)\right\}\overline{G}(2^{j-1}\omega_k)e^{-i\omega_k[(\beta_1+\beta_2)2^{j-1}-\beta_1]}, \quad (58)$$

where $\hat{S}_{2^0} f(\omega_k) = F(\omega_k)$. From the above derivation, it is obvious that the amount of phase shift is $(\beta_1 + \beta_2)2^{j-1} - \beta_1$. That is, the amount of edge shift between *f(n)* and $W_{2^j}f(n)$ is $(\beta_1 + \beta_2)2^{j-1} - \beta_1$ pixels at scale j. From Equations (39) and (41), the setting of β_1 and β_2 in our derivation process are $\beta_1 = 0$ and $\beta_2 = 1/2$. Therefore, at scale 2^j, the amount of edge shift between *f(n)* and $W_{2^j}f(n)$ is 2^{j-2} pixels. As to the 2–D wavelet transform, the amount of edge shift depends on the edge orientation. Since the maximum amount of edge shift is 2^{j-2} pixels in x and y directions, respectively. Therefore, the amount of edge shift toward any orientation should be less than $2^{j-2}\sqrt{1+1} = 2^{j-3/2}$ pixels.

From the above analysis, it is obvious that the maximum edge shift in an image at scale j is $2^{j-3/2}$ pixels. Based on the above analysis, we propose a coarse–to–fine approach to solve the edge delocalization problem. The proposed approach is described as follows. Let $E_{2^j}(m,n)$ denote the edge points detected from $W^1_{2^j}f(m,n)$ and $W^2_{2^j}f(m,n)$ by selecting the local extreme and thresholding the value of $\sqrt{|W^1_{2^j}f(m,n)|^2 + |W^2_{2^j}f(m,n)|^2}$. Since the amount of edge shift in $E_{2^1}(m,n)$ is less than $2^{1-3/2}$ pixels, the effect of delocalization is small. It means the position of each edge point in $E_{2^1}(m,n)$ is very close to its corresponding edge point in the original image. Therefore, the edge points in $E_{2^1}(m,n)$ can be used as the bases to adjust the position of each edge point in $E_{2^j}(m,n)$ for $j > 1$. Assume that the edge point to be adjusted in $E_{2^j}(m,n)$ is *P*. For each edge point *P* in $E_{2^j}(m,n)$, a target edge point Q_1 of $E_{2^{j-1}}(m,n)$ within a window mask is searched such that the distance between *P* and Q_1 is minimum and, Q_1 and *P* have the same edge direction. Here, a 5×5 search mask is used. Then, the point Q_1 is used as *P* to search the next edge point Q_2 in $E_{2^{j-2}}(m,n)$ such that the distance between Q_1 and Q_2 is minimum and their edge direction is consistent. This process is applied recursively until the final edge point Q_{j-1} in $E_{2^1}(m,n)$ is found. Finally, the position of Q_{j-1} is used as a precise location to adjust the position of *P*. In this way, all edge points in $E_{2^j}(m,n)$ for $j > 1$ will have very accurate positions.